

Construction of multi-decay pathways and realizing polymer-regulated organic smart luminescent materials

Yuxin Xiao¹ | Zongliang Xie^{1,2,3} | Mingyao Shen¹ | Hailan Wang¹ | Jiahui Li¹ | Rongjuan Huang¹ | Tao Yu^{1,2,3} 

¹Frontiers Science Center for Flexible Electronics, Xi'an Institute of Flexible Electronics & Xi'an Institute of Biomedical Materials and Engineering, Northwestern Polytechnical University, Xi'an, China

²Key Laboratory of Flexible Electronics of Zhejiang Province, Ningbo Institute of Northwestern Polytechnical University, Ningbo, China

³Research & Development Institute of Northwestern Polytechnical University in Shenzhen, Shenzhen, China

Correspondence

Tao Yu.

Email: iamtyu@nwpu.edu.cn

Funding information

Natural Science Basic Research Program of Shaanxi Province, Grant/Award Number: 2024JC-JCQN-51; National Natural Science Foundation of China, Grant/Award Numbers: 52103230, 62275217; Innovation Foundation for Doctor Dissertation of Northwestern Polytechnical University, Grant/Award Number: CX2023106; The Key Project of Ningbo Natural Science Foundation, Grant/Award Number: 2022J055

Abstract

The construction of multi-decay pathways of smart organic light-emitting materials has drawn intensive research enthusiasm owing to their substantial promise in diverse optoelectronic applications. Nowadays, numerous chemical substances have been refined to extend and enhance their intriguing luminescent properties. Nowadays, plenty of chemicals have been adapted to amplify more interesting luminescent properties. How to utilize an easy way to tune multi-decay pathways resulting in various emissions is still challenging. Here, we present a triphenylamine derivative, TPA3BP, which exhibits a variety of multi-decay pathways in different states and can exhibit thermally activated delayed fluorescence in both the polydimethylsiloxane and crystalline state, but also achieve room temperature phosphorescence by embedding it into the poly (methyl methacrylate) (PMMA) and polyvinyl pyrrolidone matrix. The multi-decay luminescence can be attributed to the dual effect arising from the $n-\pi^*$ transition of TPA3BP and the regulation of molecular transition pathways within the matrix environment. This intriguing phenomenon highlights the combined influence of TPA3BP's electronic transitions and the influence of the polarity and rigidity of the surrounding matrix on the observed characteristics. This advancement has widened the structural possibilities for multi-decay luminescent materials, enabling their targeted synthesis for future applications, such as information encryption and smart anti-counterfeiting.

KEYWORDS

host-guest materials, room temperature phosphorescence (RTP), smart counterfeiting materials, thermally activated delayed fluorescence (TADF)

Yuxin Xiao and Zongliang Xie authors contributed equally.

This is an open access article under the terms of the [Creative Commons Attribution](https://creativecommons.org/licenses/by/4.0/) License, which permits use, distribution and reproduction in any medium, provided the original work is properly cited.

© 2024 The Author(s). FlexMat published by John Wiley & Sons Australia, Ltd on behalf of Nanjing University of Posts & Telecommunications.

1 | INTRODUCTION

Smart organic luminescent materials with the ability to efficiently respond to external stimuli (temperature, humidity, stress, pH, electric or magnetic field, light or chemical substances, etc.) have attracted immense interest owing to their substantial promise in diverse optoelectronic applications, including optical data recording, storage, and anti-counterfeiting as well as flexible electronic.^{1–10} In particular, great progress has been made in the construction of multi-decay pathways to realize smart luminescence. For instance, visible-near infrared dual emission materials that could be tuned under different excitations have been developed recently, showing an important advance in the field of organic intelligent luminescent materials to enhance the security of encrypted information and anti-counterfeiting.¹¹ Moreover, Chen et al. propose to engineer the resonance linkage between flexible chain and phosphor units to regulate the activation energy of resonance variation, which could further realize on-demand controllable organic ultralong room temperature phosphorescence (RTP).¹² These approaches have been noted for their diverse luminescent responses to various stimuli, yet their practical application is hindered by complex preparation processes, high costs, and systematic material design challenges.

Host/guest doping systems provide a robust supramolecular approach to facilitate the creation of multi-decay pathways.^{13–15} This is achieved by leveraging the rigid environment and precise energy levels offered by the host materials, leading to the efficient generation and stabilization of long-lived triplet excitons. The controlled manipulation of photophysical properties within the host/guest system holds significant promise for a wide range of applications, capitalizing on its versatility and tunability.^{16–18} In the previous work of our team, a series of multi-host/guest materials with various microenvironments and tunable energy level platforms were developed to achieve lifetime-encoding ultralong organic phosphorescence.^{19–20} Recently, researchers have also paid more attention to manipulating radiative decay channels by doping guests into polymers. Typically, polymers demonstrate outstanding mechanical strength, favorable toughness, high processability, cost-effectiveness, and an array of other advantageous properties.^{21–22} Regulating the mutual competition of multiple transition channels is an effective way to efficiently construct multi-decay emissions. Introducing elements containing lone pair electrons, such as N, O, F, etc., can effectively enhance the spin-orbit coupling (SOC) between the singlet and triplet states, thereby promoting intersystem crossing (ISC) processes. Besides, stabilizing

the lowest excited triplet state (T_1) and reducing the nonradiative decay and quenching processes by doping into various matrices or introducing polymer chains. However, most studies focused on the tuning strategy of RTP materials. Integrating multi-decay luminescence mechanisms into a system is a complex and challenging task. When considering only two excited states, T_1 and S_1 , it becomes evident that simultaneously satisfying the intrinsic distribution of energy levels is difficult. Moreover, in a complex solid-state environment, the uncontrolled competition between ISC and reverse ISC processes further complicates the situation. Based on this, the construction of rational multi-decay channels by developing abundant polymeric environments is extraordinarily important but seldom reported.

Donor-acceptor (D-A) type organic luminescent materials, which may typically have intramolecular charge transfer (ICT) and intermolecular charge transfer mechanisms, are an important class of organic smart luminescent materials with tunable multi-decay channels,^{23–24} such as RTP and thermally activated delayed fluorescence (TADF), that can fully utilize triplet state energy. In particular, nitrilotris(benzene-4,1-diyl)tris(phenylmethanone) (TPA3BP) composed of triphenylamine (TPA) (D) and benzophenone (A) was designed and prepared. Previous studies have identified an equilibrium between intramolecular and intermolecular charge transfer caused by the formation of intermolecular C-H...O hydrogen bonds that lead to dual emission. Moreover, it has been reported that the synergistic effect between carbonyl groups and heteroatoms promotes the hybrid $n-\pi^*$ and $\pi-\pi^*$ transition to promote the SOC effect, thus further promoting the ISC process to populate triplet states.²⁵ TPA3BP not only shows TADF features in the crystalline and low-polarity polydimethylsiloxane (PDMS) matrix but also achieves RTP by embedding it into the high polarity poly(methyl methacrylate) (PMMA) and polyvinyl pyrrolidone (PVP) matrix (Figure 1). Surprisingly, TPA3BP@PDMS exhibits remarkable thermal-sensitive fluorescence characteristics with temperature variations of 20–40°C, rendering it highly suitable for body temperature sensing applications. Cyan afterglow at room temperature could be observed upon TPA3BP doping into PMMA and PVP with higher rigidity due to the suppressed non-radiation transition progresses. Among them, TPA3BP@PMMA exhibited photo-induced RTP, while TPA3BP@PVP showed direct RTP. This study presents a compelling case demonstrating the manipulation of the radiative decay channel through fine-tuning the guests' microenvironments, effectively restricting their vibration and rotation to realize multi-channel luminescence.

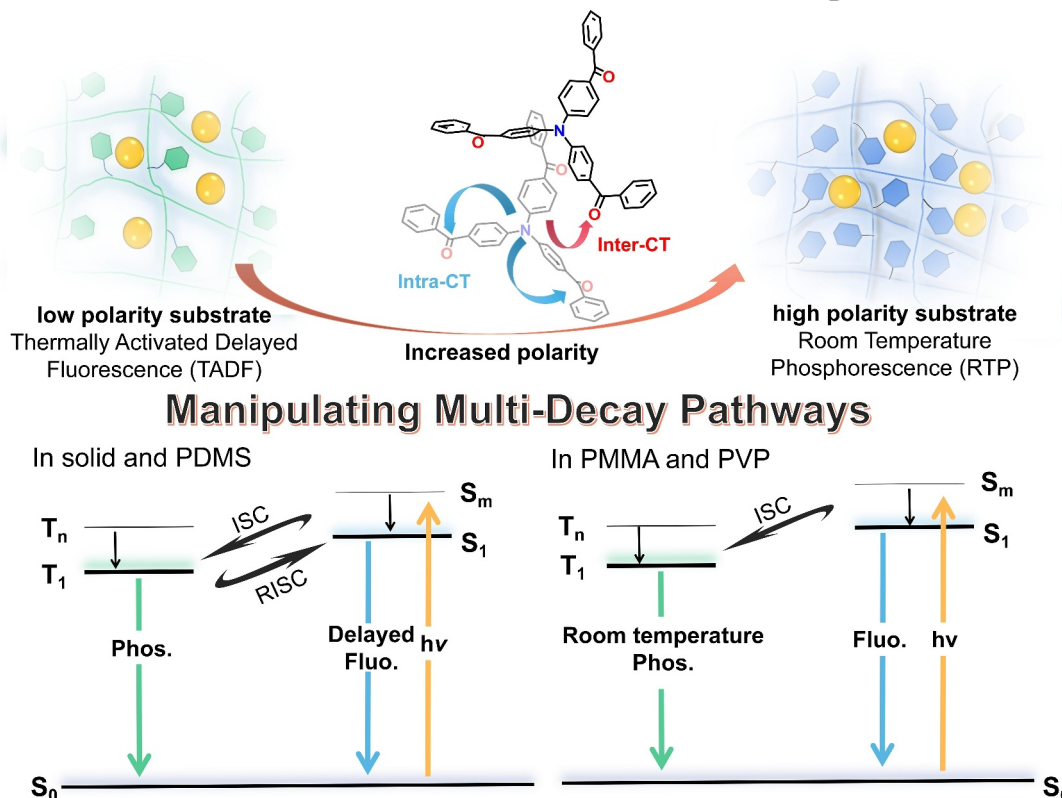


FIGURE 1 Construction of Multi-decay Pathways like RTP and TADF by realizing polymer regulated smart organic light-emitting materials. RTP, room-temperature phosphorescence.

2 | RESULTS AND DISCUSSIONS

The organic smart luminescent molecule TPA3BP was designed by constructing three benzophenone (BP) groups from TPA groups and synthesized by a one-step Friedel-Crafts acylation reaction. The specific synthetic process is described in detail in the experimental section of Scheme S1. Chemical structure and purity were further confirmed by nuclear magnetic resonance, high-resolution mass spectrometry (Figures S1–S3, Supporting Information), and X-ray crystallographic analysis (Tables S5–S7, Figure S17).

To investigate the photophysical properties of TPA3BP at the molecular level, we initially recorded its UV-vis absorption and fluorescence spectra in a dilute methyltetrahydrofuran (2Me-THF, 1×10^{-5} M) solution at room temperature. The absorption spectrum shows characteristic $\pi-\pi^*$ and $n-\pi^*$ transitions with the main band at 372 nm. The solvent effect is a prominent feature of ICT materials, which can be confirmed by absorption and emission spectra (Figures S4 and S5). The emission line shape of TPA3BP is structureless at room temperature, with a peak located at 439 nm, giving rise to an intense blue emission. Notably, due to its ICT nature, its emission band is actually susceptible to environmental

polarity. As shown in Figure S5, with substantially increasing solvent polarity from low-polar toluene to high-polarity dimethyl formamide, its PL spectra undergo a variation with a redshift up to 68 nm. The PL spectra of TPA3BP show a positive solvatochromism effect. This provides an opportunity to modulate its emission spectrum based on environmental factors.

Concentration-dependent emission spectra of TPA3BP were measured in toluene solution to demonstrate the source of lower energy emission bands. As shown in Figure 2B, when the concentration of TPA3BP is lower than 1.0×10^{-3} mol L⁻¹, only the higher energy emission band can be observed. This higher energy emission band around 420 nm is assigned to the ICT emission for its sensibility to solvent polarity as illustrated before. The lower energy emission band (maxima ≈ 560 nm) appears when the concentration reaches 1.0×10^{-3} mol L⁻¹ which originates from intermolecular charge transfer. To further investigate intermolecular charge transfer emission and to verify the presence of intermolecular hydrogen bonds, a trace amount of methanol was gradually added to benzene solutions to weaken the intermolecular hydrogen bonding. Figure 2C shows the changes in the emission spectra of TPA3BP in benzene solution (10.0 mL, 1.0×10^{-3} mol L⁻¹) after the

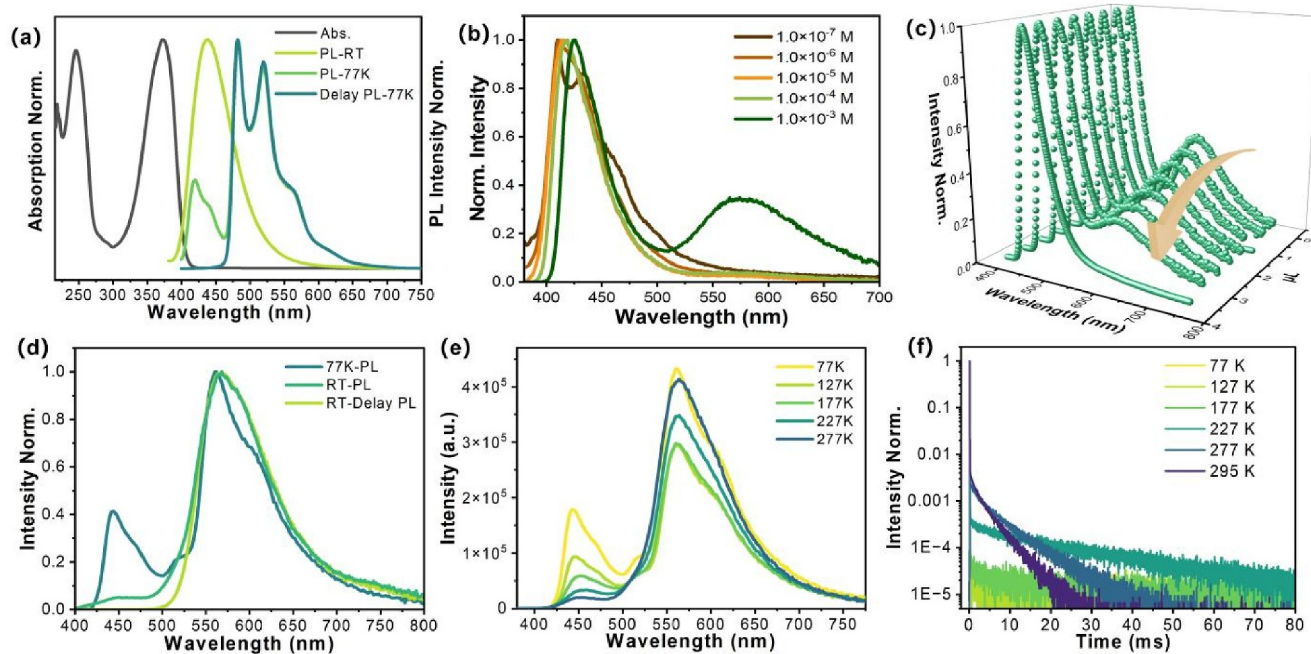


FIGURE 2 (A) UV-vis absorption, PL, and delayed PL spectra of TPA3BP (1 μM) in 2-Methyltetrahydrofuran solution at 295 K (RT) and 77 K; the gate-controlled delay time was 8 ms ($\lambda_{\text{ex}} = 365$ nm). (B) Concentration-dependent PL spectra of TPA3BP in toluene solution ($\lambda_{\text{ex}} = 365$ nm). (C) Changes in PL spectra of TPA3BP by gradual addition of methanol per 0.5 μL in toluene (10.0 mL, 1×10^{-3} mol/L, $\lambda_{\text{ex}} = 365$ nm). (D) The PL spectra and delay PL spectra of TPA3BP (crystalline) at room temperature and 77 K ($\lambda_{\text{ex}} = 365$ nm). (E) Temperature-dependent steady-state PL spectra and (F) decay curves (at 560 nm) of TPA3BP (crystalline) ($\lambda_{\text{ex}} = 365$ nm). PL, photoluminescent.

gradual addition of methanol (0.5 μL per time). As anticipated, the intensities of the lower energy emission bands decrease and are finally quenched with the step-wise addition of methanol. Therefore, by controlling the formation or destruction of the intermolecular hydrogen bonding, the emission properties of these compounds can easily be tuned. With respect to TPA3BP, the emission colors can be tuned from (0.31, 0.24) to (0.17, 0.11) by the addition of methanol to the toluene solution (Figure S6). To gain a more comprehensive insight into the triplet character, variations in luminescence at 77 K were also investigated. The phosphorescence spectrum of TPA3BP is well resolved and shows vibrational characteristics, and the phosphorescent peaks of TPA3BP showed structured emissions at 482, 520, and 562 nm.

To further investigate the properties of the intermolecular charge transfer emission, temperature-dependent emission studies were performed in the crystalline state. The crystalline samples of TPA3BP present emission peaks at 444 and 562 nm at 77 K (Figure 2D), whose emission band at 444 nm is very close to that in its 2Me-THF solution. At room temperature, the PL spectrum of TPA3BP peaked at 562 nm with a lifetime of 11.59 ns (Figure S7b). Temperature-dependent emission spectra of TPA3BP in the crystalline state were also performed, as shown in Figure 2E. The time-resolved decay curves showed that the

delayed component unusual increased with increasing temperature from 77 to 177 K, which could be attributed to the enhanced nonradiative transition and the influence of the emergence of a phosphorescence component.^{26–28} Besides, the results clearly show that TPA3BP crystal exhibits stronger prompt and more negligible delayed fluorescence components when the temperature decreases, which are consistent with TADF characteristics (Figure 2F). Therefore, the lower energy emission band is assigned to intermolecular charge transfer emission with TADF characteristics, which is similar to TADF emission described in previous studies.²⁹

To better understand the emission mechanism, we determined the exact molecular conformation by single-crystal diffraction analysis. Yellow crystal TPA3BP was obtained by recrystallization from mixed dichloromethane/n-hexane solvent systems. From the X-ray diffraction (XRD) analyses, it was found that the molecules in the single crystals of TPA3BP are packed based on the P21n space group. TPA3BP exhibits a propeller-like structure due to the non-coplanar orientation of its three benzene rings within the TPA skeleton. The dihedral angles between these rings are notably large (65.59°, 70.11°, and 73.59°), making them nearly orthogonal to the TPA group plane (dihedral angle of 73.59°) within the single crystal structures. Various intermolecular interactions,

such as C–H $\cdots\pi$, C–H \cdots O, and π – π interactions, are evident in the crystal structure. Consequently, the tight stacking creates a rigid environment, which should promote luminescence with a high quantum efficiency of 19.9% in the solid state. Moreover, C–H \cdots O intermolecular hydrogen bonding (Figure 3A) was formed between all the carbonyl and the nearby benzene rings from another TPA structure with distances of 2.566 Å, 2.651 Å, and 3.159 Å. These intermolecular hydrogen bonds facilitate proximity between donor and acceptor moieties in separate molecules within the aggregated state. Thus, intermolecular charge transfers may occur after excitation. From the discussions above, it is highly likely that the fluorescence peak at 562 nm originated from intermolecular CT. Consequently, the tight stacking creates a rigid environment, which should promote luminescence with high quantum efficiency in the crystalline state.

To further explore the inherited mechanism of diverse photophysical properties and establish the structure-property relationship, time-dependent density functional theory calculations were carried out on the G09 program at B3LYP/6-311G* set based on the single crystal structure.³⁰ Orbital distributions and calculated the highest occupied molecular orbital (HOMO), the lowest unoccupied molecular orbital (LUMO), singlet and triplet energy levels, bandgaps, and ΔE_{ST} for TPA3BP based on a single crystalline state, as illustrated in Table S1. For TPA3BP monomer, the electron density was localized mostly on TPA fragments in the HOMO and the BP fragment in the LUMO, which is typical for compounds with ICT. A different situation was found for the TPA3BP dimer. As illustrated in Table S2, according to natural transition orbital analysis, the S_0 – S_1 transition reveals a distinct intermolecular CT, primarily located on the BP unit of the neighboring molecule.^{31–32} For TPA3BP dimer

(Table S3), the HOMO and LUMO are located in different molecules for the intermolecular CT emission.

Based on the photophysical properties and calculated results, a simplified Jablonski diagram is proposed in Figure 3B. Upon UV light excitation, TPA3BP was advanced to the excited monomer and dimer states (named S_1^M and S_1^D). Additional decay pathways, including nonradiative decay to the ground state and the process of ISC, leading to the formation of the excited triplets T_1^M and T_1^D , are also present. However, T_1^M -state exciton could initially be quenched by the surrounding molecular oxygen and undergo deactivation pathways such as triplet-triplet annihilation. To efficiently utilize the corresponding triplet excitons, a polymer matrix with different rigidities can be introduced to adjust luminescence propensities. As reported before, a rigid polymer matrix can be introduced to effectively suppress the molecular motion and inhibit both ISC and other non-radiative transitions. Therefore, polymers could be utilized as the matrix to construct multi-decay pathways of smart organic light-emitting materials.

In this work, polymers for the construction of multi-decay pathways and realizing polymer-regulated smart organic light-emitting materials were tested to be practicable. To build different host energy levels and suppress the non-radiation process, three polymers with different polarities and rigidities were chosen to further construct doped materials, namely, PDMS, PMMA and PVP. All these hosts are directly purchased commercially and used. None of them show RTP or thermal-sensitive luminescence properties, but all hosts have good solubility and membrane abilities. PVP and PMMA were reported as rigid matrices for effectively suppressing the molecular motion to inhibit both reverse ISC and other nonradiative transitions, thereby providing a feasible way

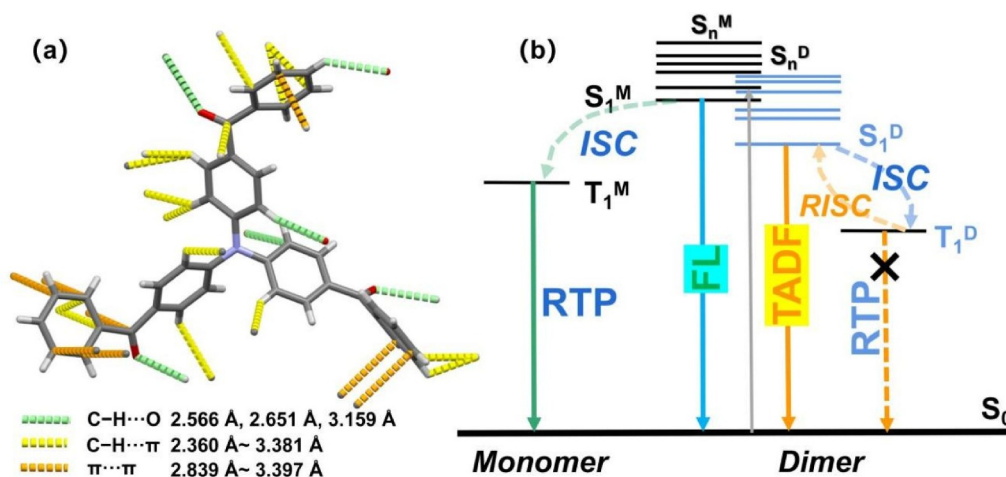


FIGURE 3 (A) Intermolecular hydrogen bonds in the crystal of TPA3BP. (B) Strategy to construct efficient TADF and RTP triggered by intermolecular CT process.

for RTP emission. TPA3BP@PMMA and TPA3BP@PVP doped films with 1:1000 weight ratios were prepared to test materials with the multi-luminescence property, and the detailed preparation processes are presented in supporting information. The steady-state absorption and emission spectra of TPA3BP (Figure S8 and Figure 4B) were measured in different polarities and rigidities of polymers PDMS, PMMA and PVP. Three absorption peaks (approximately 360–385 nm) are located on the blue side, which are independent of the host polarity. However, the absorption peak centered at ~369 nm for TPA3BP in n-hexane shows a redshift as the host polarity increases because the lone electron pairs of nitrogen atoms can be particularly stabilized by the polar host.³³ The absorption peak is centered at 362 nm in PDMS, 372 nm in PMMA and 382 nm in PVP, respectively. Therefore, the polarity of the referred polymer can be

deduced, presumably with PVP being the largest, PMMA the second largest, and PDMS the smallest. Besides, we also studied the PL and delay PL spectra of TPA3BP in various polymer doped films are studied to reveal the energy level of TPA3BP in the polymer matrices, as shown in Figure S9 and Table S4.

Since neither TPA3BP powders nor polymeric matrices emit RTP, it is evident that RTP of the TPA3BP doped polymer films is from dispersed TPA3BP molecules encapsulated in rigid PMMA and PVP matrices. The polar environment of the polymer inhibits effectively the formation of intermolecular hydrogen bonds (Figure S10), therefore there was no corresponding formation of intermolecular CTs, which also resulted in the RTP only happening in monomers. Microstructures of doped polymers were further investigated by XRD to elucidate the RTP mechanism. The TPA3BP@PMMA

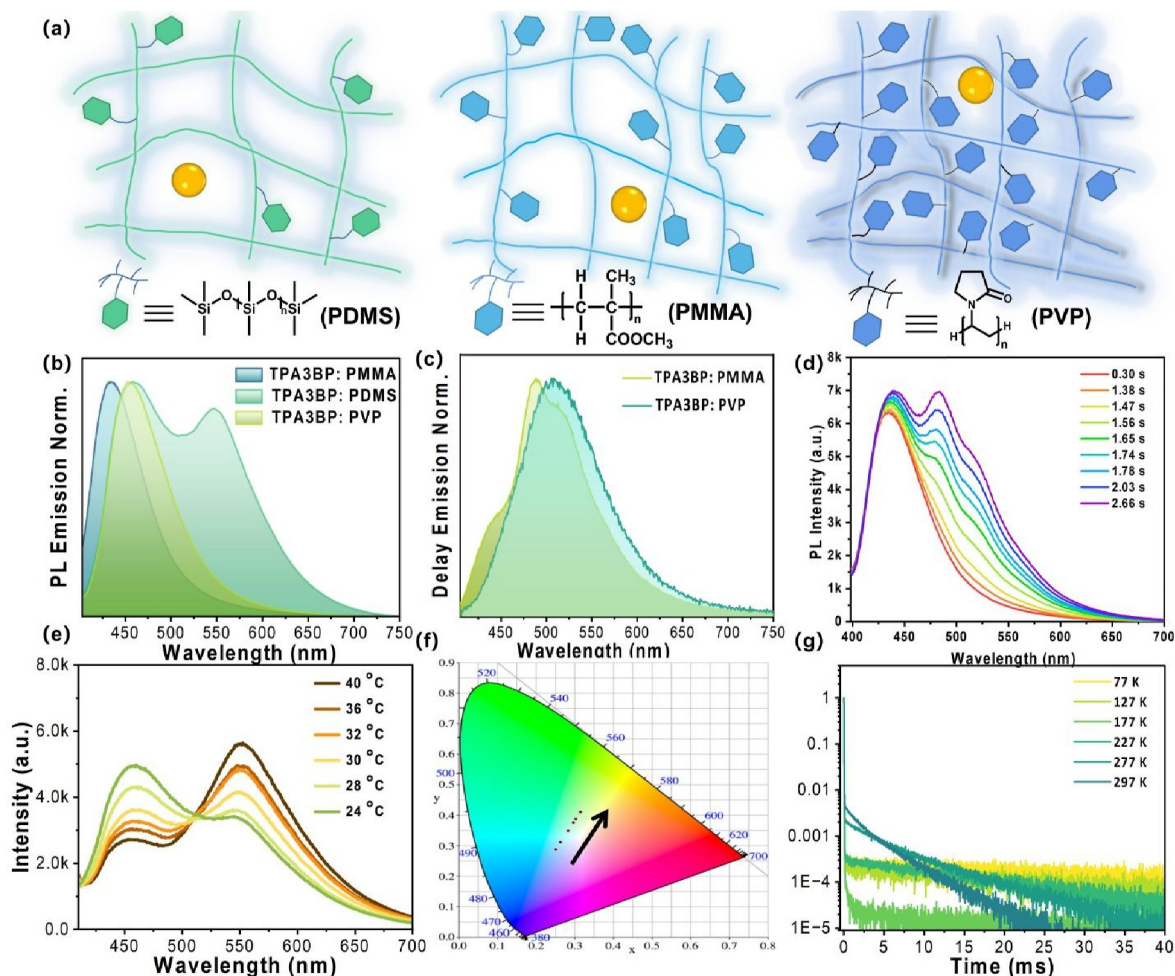


FIGURE 4 (A) Schematic illustration of the structure of the TPA3BP@PDMS, TPA3BP@PMMA and TPA3BP@PVP doped materials. (B) Normalized PL spectra of doped materials under 365 nm excitation. (C) Normalized delay PL spectra of doped materials (delay 8 ms) under 365 nm excitation. (D) Time-dependent steady-state PL spectra of TPA3BP@PMMA upon 365 nm excitation at room temperature. (E) Temperature-dependent emission spectra of TPA3BP@PDMS with (F) CIE color coordinates. (G) Decay curves of TPA3BP@PDMS at different temperatures (Ex.: 365 nm). PL, photoluminescent.

doped polymers show a distinct diffraction peak at 14° similar to PMMA, indicating that they have the similar crystalline structure (Figures S11 and S12) to pristine PMMA. The diffraction peaks from TPA3BP crystals are not observed in the XRD patterns of the doped polymers, demonstrating that TPA3BP molecules are individually distributed in the doped polymer films. TPA3BP@PMMA and TPA3BP@PVP doped films show PL emissions around 443 nm with similar spectra, which show guest characteristics in a unimolecular state, as shown in Figures 2A and 4B. PMMA was reported as an oxygen permeable material that could be utilized by long-term irradiation. With sustaining irradiation of UV light for 2.66 s, the PL emission intensity increased to its maximum, and the arousal of the phosphorescence emission peak at 484 nm gradually boosted (Figure 4D). Therefore, the emission color switched from blue to yellow-green of TPA3BP@PMMA which should be attributed to the arousing phosphorescence emission under sustaining UV irradiation. As a result, the delayed PL spectrum of TPA3BP@PMMA reveals the existence of persistent emission around 489 nm with a lifetime of 67.42 ms which could not be directly seen. This room-temperature phosphorescence phenomenon awakened by photoexcitation is often referred to as light-induced RTP.^{34–37}

As for TPA3BP@PVP doped film, a fluorescence peak at 455 nm was recorded when excited with light at 365 nm. In delay emission spectra (Figure 4C, delay time = 8 ms), TPA3BP@PVP exhibited a strong phosphorescence emission at 506 nm with a 59.59 ms lifetime. In this system, PVP can inhibit nonradiative transition through rigid environments and hydrogen bonding interactions between the substrate and TPA3BP. Thus, the RTP property could be directly exhibited in the TPA3BP@PVP. The differences in delay PL emission between TPA3BP@PMMA and TPA3BP@PVP revealed similar but different energy transfer processes due to different excited state configurations of TPA3BP deriving from diverse polymeric environments.

The above results demonstrate T_1^M could be strongly stabilized by the rigid and high polar polymer matrix and exhibit a characteristic green RTP. Incorporation of TPA3BP into a rigid matrix is an effective way to boost RTP emissions. Nevertheless, in a low-polarity polymer matrix like PDMS, TPA3BP exhibits TADF properties similar to the aggregated state without RTP emission. The emission of TPA3BP@PDMS show different properties from those of TPA3BP@PMMA and TPA3BP@PVP. TPA3BP@PDMS exhibited distinct dual emissions, as shown in Figure 4E and Figure S13. The doped polymeric films were made by the method reported in the support information. For the chosen flexible matrix PDMS,

TPA3BP@PDMS exhibits a distinct aggregate state property in this matrix, possibly due to its presence in the form of dimers in the matrix. For crystalline TPA3BP, combined with the actual experimental results, the emission peak caused by intermolecular charge transfer shows obvious TADF properties, while the intrinsic material single-molecule fluorescence peak is fluorescence. Two emission sources with different temperature sensitivities contribute to the difference in luminescence of TPA3BP@PDMS at different temperatures.

The PL intensity of emission at 460 nm decreases with the temperature increasing from 77 to 300 K but the yellow emission band at 560 nm increases. Temperature-dependent luminescence shows cool white light at low temperatures, and with the increase in temperature, the TADF peak is further activated, and the material shows obvious emission changes from white light (0.26, 0.31) to warm white light (0.32, 0.41) to yellow light (Figure 4F). Based on the similarity solution principle, the small polarity and rigidity of PDMS caused TPA3BP exhibit TADF, like in the aggregation state. The emission peak at 560 nm disappeared when the doping concentration was reduced to 1: 10 000 (Figure S13). The emission at 560 nm shows similar spectra with the intermolecular hydrogen bonds between TPA3BP and nearby TPA3BP as mentioned above, which also exhibit TADF. Temperature-dependent emission studies were performed for the lower energy emission band of the TPA3BP@PDMS thin film (Figure 4G and Figure S14). The results clearly show that TPA3BP@PDMS thin film exhibits TADF characteristics similar to the TADF of crystalline TPA3BP.

Overall, the experimental results suggest that the decay pathways of TPA3BP in the polymer host may be influenced by the polarity of the polymeric matrix. Besides, the differences of the oxygen permeability properties of the polymers also resulting in both of the TPA3BP@PDMS and TPA3BP@PVP did not exhibit obvious light-induced RTP like TPA3BP@PMMA as shown in Figure S15. To our delight, the results show the agreement with design strategy that when doping into high polarity and rigidity host polymers, evident RTP could be observed. However, doped materials when using flexible substrates like PDMS, RTP did not exist. This phenomenon also explains that the PL spectra of TPA3BP in PMMA and PVP do not show the emission peak of its own intermolecular hydrogen bonds (Figure S16) due to the formation of hydrogen bonds with the polar host materials.

Considering the switchable PL properties of TPA3BP-based doping polymers, it can be applied to anticounterfeiting and information encryption. We developed a series of patterns to visualize their characteristics, as shown in Figure 5A. The pattern of TPA3BP@PDMS is poured into silicone molds and dried at 70°C for a day,

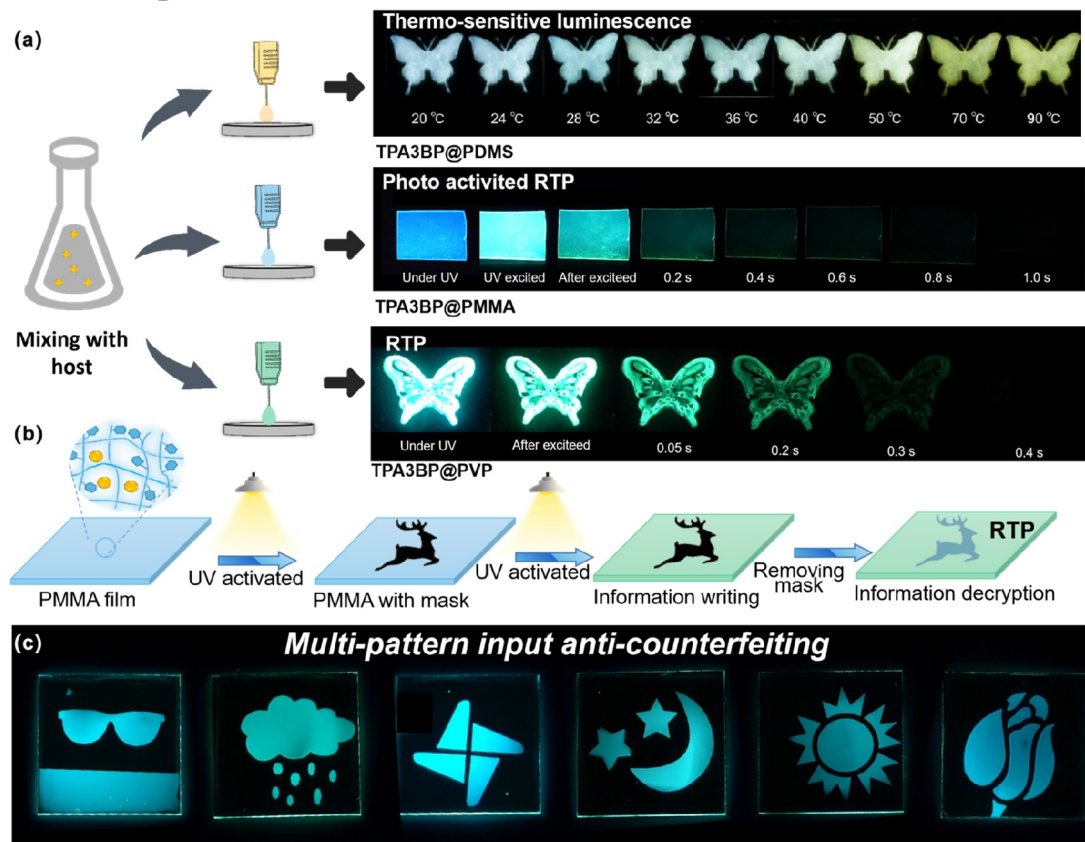


FIGURE 5 Application of doping polymeric materials in anti-counterfeiting and information encryption. (A) Photographs of TPA3BP@PDMS patent at various temperatures and RTP materials like TPA3BP@PMMA and TPA3BP@PVP. (B) Applications of TPA3BP@PMMA in information encryption and (C) multi-pattern input anti-counterfeiting photographs.

producing a butterfly-shaped label with different PL visualizations under various temperatures. The TPA3BP@PMMA film exhibited blue emission under 365 nm UV irradiation, and no RTP could be observed after ceasing the UV light at the beginning. However, when the film was excited for several seconds with UV light, the blue emission of the film changed into a cyan emission, and the cyan RTP can be seen after stopping UV excitation. After 365 nm activation, the PLQY has been significantly improved, from 5.1% to 21.4%. The pattern of TPA3BP@PVP could exhibit cyan RTP under 365 nm UV irradiation with PLQY up to 27.8%.

Advanced information encryption and decryption could be realized by making use of the UV irradiation responsive RTP properties of doping PMMA systems.^{38–42} We took advantage of TPA3BP@PMMA film to serve as information encryption paper, and the UV light was used as the ink to write or paint different information within different regions. As illustrated, the encrypted pattern was input by using the mask. In the absence of ultraviolet light, the written information is unreadable to the naked eye. However, after removing the mask, the film exhibited cyan emission with the information deer under 365 nm UV irradiation (Figure 5B). After removing UV irradiation for

different durations, this pattern is changed into a green running deer. As shown in Figure 5C, by putting a photo-mask with various patterns on the film surface, the input pattern turns green after continuous UV irradiation. Similarly, the pattern sunglasses, clouds and rain, windmill, moon and stars, sun and rose were drawn with UV light, which all exhibit bright cyan emission after stopping UV excitation. Moreover, the resulting picture could be retained for several seconds due to the unique RTP properties. Afterward, the pattern could be cleared via consistent illumination of the entire film, thus achieving the role of encryption information being erased, to achieve the purpose of decoration and encryption. These preliminary results demonstrate that TPA3BP has great potential applications in advanced anti-counterfeiting and information encryption technologies.

3 | CONCLUSION

In conclusion, we have proposed a convenient strategy to achieve multi-decay pathways based on doping TPA3BP into different polymers, and finally, we have successfully realized polymer regulated smart organic light-emitting

material. Polymers like PMMA and PVP with distinct rigidity, triplet energy level, and oxygen permeation result in the cyan RTP of doping materials, which did not exist in the TPA3BP. Excitingly, PMMA films of TPA3BP demonstrate photo-induced RTP due to consuming oxygen under UV irradiation, while the RTP of TPA3BP@PVP could directly exhibit no excitation. In addition, applying flexible substrate PDMS could rationally tune the dual-emission at different temperatures from cold-white to yellow. This handy approach can also provide a controlled temperature-sensitive material to build accurate temperature-identifying structures and ideal models. Based on this strategy, more accurate dynamic anticounterfeiting with RTP, TADF, temperature sensitive emissions can be easily achieved based on selecting different polymers, which may open a new research direction in organic excitons regulation.

3.1 | Experimental section

CCDC 2281471 contain the supplementary crystallographic data for this paper. These data can be obtained free of charge from The Cambridge Crystallographic Data Center.

AUTHOR CONTRIBUTIONS

Yuxin Xiao: Investigation; writing – original draft. **Zongliang Xie:** Investigation; writing – review & editing. **Mingyao Shen:** Investigation. **Hailan Wang:** Writing – review & editing. **Jiahui Li:** Investigation. **Rongjuan Huang:** Writing – review & editing. **Tao Yu:** Conceptualization; investigation; supervision; writing – review & editing.

ACKNOWLEDGMENTS

Yuxin Xiao and Zongliang Xie contributed equally to this work. The authors gratefully acknowledge the financial support from the NSF of China (62275217, 52103230), Natural Science Basic Research Program of Shaanxi Province (2024JC-JCQN-51), The key project of Ningbo Natural Science Foundation (2022J055) and Innovation Foundation for Doctor Dissertation of Northwestern Polytechnical University (CX2023106).

CONFLICT OF INTEREST STATEMENT

The authors declare no conflict of interests.

DATA AVAILABILITY STATEMENT

The data that support the plots within this paper and other findings of this study are available from the corresponding author upon reasonable request.

ORCID

Tao Yu  <https://orcid.org/0000-0002-2855-3104>

REFERENCES

1. Y. Wang, H. Wu, W. Hu, J. F. Stoddart, *Adv. Mater.* **2022**, *34*, 2105405.
2. W. K. Haug, E. M. Moscarello, E. R. Wolfson, P. L. McGrie, *Chem. Soc. Rev.* **2020**, *49*, 839.
3. Z. Wang, L. Gao, Y. Zheng, Y. Zhu, Y. Zhang, X. Zheng, C. Wang, Y. Li, Y. Zhao, C. Yang, *Angew. Chem. Int. Ed.* **2022**, *61*, e202203254.
4. Y. Zhang, S. Zhang, G. Liu, Q. Sun, S. Xue, W. Yang, *Chem. Sci.* **2023**, *14*, 5177.
5. J. Li, Y. Wu, X. Gong, *Chem. Sci.* **2023**, *14*, 3705.
6. Z. Man, Z. Lv, Z. Xu, M. Liu, J. He, Q. Liao, J. Yao, Q. Peng, H. Fu, *J. Am. Chem. Soc.* **2022**, *144*, 12652.
7. D. Yan, Z. Wang, Z. Zhang, *Acc. Chem. Res.* **2022**, *55*, 1047.
8. C. C. Kenry, B. Liu, *Nat. Commun.* **2019**, *10*, 2111.
9. X. Yan, H. Peng, Y. Xiang, J. Wang, L. Yu, Y. Tao, H. Li, W. Huang, R. Chen, *Small* **2022**, *18*, 2104073.
10. L. Ma, X. Ma, *Sci. China. Chem.* **2023**, *66*, 304.
11. Y. Li, J. Sun, M. Chen, S. Miao, M. Liu, Y. Ma, G. Wang, X. Gu, B. Z. Tang, *Adv. Funct. Mater.* **2022**, *32*, 2205494.
12. Y. Tao, C. Liu, Y. Xiang, Z. Wang, X. Xue, P. Li, H. Li, G. Xie, W. Huang, R. Chen, *J. Am. Chem. Soc.* **2022**, *144*, 6946.
13. J. Chen, F. Lin, G. Liang, H. Huang, T. Qin, Z. Yang, Z. Chi, *J. Mater. Chem. C* **2023**, *11*, 6290.
14. J. Wang, Y. Yang, X. Sun, X. Li, L. Zhang, Z. Li, *Light. Sci. Appl.* **2024**, *13*, 35.
15. N. Xue, H. Zhou, Y. Han, M. Li, H. Lu, C. Chen, *Nat Commun* **2024**, *15*, 1425.
16. H. Dong, C. Zhang, J. Yao, Y. Zhao, *Aggregate* **2021**, *2*, e103.
17. M. Du, Y. Shi, Q. Zhou, Z. Yin, L. Chen, Y. Shu, G. Sun, G. Zhang, Q. Peng, D. Zhang, *Adv. Sci.* **2022**, *9*, 2104539.
18. X. Chen, W. Dai, X. Wu, H. Su, C. Chao, Y. Lei, J. Shi, B. Tong, Z. Cai, Y. Dong, *Chem. Eng. J.* **2021**, *426*, 131607.
19. Z. Xie, X. Zhang, H. Wang, H. Sun, M. Dong, L. Ji, Z. An, T. Yu, W. Huang, *Nat. Commun.* **2021**, *12*, 3522.
20. R. Huang, Y. He, J. Wang, J. Zou, H. Wang, H. Sun, Y. Xiao, D. Zheng, J. Ma, T. Yu, W. Huang, *Nat. Commun.* **2024**, *15*, 1596.
21. J. Guo, C. Yang, Y. Zhao, *Acc. Chem. Res.* **2022**, *55*, 1160.
22. Y. Gong, J. Yang, M. Fang, Z. Li, *Cell Rep. Phys. Sci.* **2022**, *3*, 100663.
23. J. Fang, P. Li, X. Xue, H. Li, D. Cui, J. Zhang, Y. Wang, T. Debnath, Y. Jie, W. Huang, R. Chen, *Chem. Mater.* **2023**, *35*, 6405.
24. T. Zhang, Y. Xiao, H. Wang, S. Kong, R. Huang, V. Ka-Man Au, T. Yu, W. Huang, *Angew. Chem. Int. Ed.* **2023**, *62*, e202301896.
25. X. Han, K. Chen, Y. Lei, J. Huang, S. Wei, Z. Cai, H. Wu, M. Liu, X. Huang, Y. Dong, *ACS Mater. Lett.* **2022**, *4*, 1764.
26. L. Chen, C. Li, E. Fu, M. Li, Y. Kuboi, Z. Li, Z. Chen, J. Chen, X. Liu, X. Tang, L. Frédéric, F. Maurel, C. Adachi, F. Mathevet, S. Zhang, *ACS Mater. Lett.* **2023**, *5*, 1450.
27. Y. Wang, M. Gao, J. Ren, J. Liang, Y. Zhao, M. Fang, J. Yang, Z. Li, *Mater. Chem. Front.* **2023**, *7*, 1093.
28. X. Wei, Y. Chen, R. Duan, J. Liu, R. Wang, Y. Liu, Z. Li, Y. Yi, Y. Yamada-Takamura, P. Wang, Y. Wang, *J. Mater. Chem. C* **2017**, *5*, 12077.
29. K. Goushi, K. Yoshida, K. Sato, C. Adachi, *Nat. Photonics* **2012**, *6*, 253.

30. I. M. Khan, F. Naaz, S. Shakya, M. Islam, A. Khan, M. Ahmad, *J. Mol. Liq.* **2024**, 339, 124412.
31. C. Wang, Y. Zhang, Z. Wang, Y. Zheng, X. Zheng, Y. Huang, Z. Lu, *J. Mater. Chem. C* **2020**, 8, 11603.
32. T. Lu, F. Chen, *J. Comput. Chem.* **2012**, 33, 580.
33. W. Zhang, J. Kong, R. Z. An, J. Zhang, Y. Zhou, L.-S. Cui, M. Zho, *Aggregate* **2023**, 5, e416.
34. C. Wang, Y. Zhang, Z. Wang, Y. Zheng, X. Zheng, L. Gao, Q. Zhou, J. Hao, X. Pi, Q. Li, C. Yang, Y. Li, K. Wang, Y. Zhao, *Adv. Funct. Mater.* **2022**, 32, 2111941.
35. L. Yue, Q. Sun, Y. Zhang, Y. Wang, S. Cui, H. Zhang, S. Xue, W. Yang, *Chem. Eng. J.* **2022**, 433, 134307.
36. H. Zheng, Z. Zhang, S. Cai, Z. An, W. Huang, *Adv. Mater.* **2024**, 2311922.
37. Y. Zheng, K. Arkin, Y. Bei, X. Ma, Q. Shang, *Matter* **2023**, 6, 4339.
38. X. Wang, Y. Sun, G. Wang, J. Li, X. Li, K. Zhang, *Angew. Chem. Int. Ed.* **2021**, 60, 17138.
39. X. Yang, G. I. N. Waterhouse, S. Lu, J. Yu, *Chem. Soc. Rev.* **2023**, 52, 8005.
40. X. Dou, X. Wang, X. Xie, J. Zhang, Y. Li, B. Tang, *Adv. Funct. Mater.* **2024**, 2314069.
41. Q. Chen, L. Qu, H. Hou, J. Huang, C. Li, Y. Zhu, Y. Wang, X. Chen, Q. Zhou, Y. Yang, C. Yang, *Nat. Commun.* **2024**, 15, 2947.
42. L. Zhou, J. Song, Z. He, Y. Liu, P. Jiang, T. Li, X. Ma, *Angew. Chem. Int. Ed.* **2024**, 63, e202403773.

SUPPORTING INFORMATION

Additional supporting information can be found online in the Supporting Information section at the end of this article.

How to cite this article: Y. Xiao, Z. Xie, M. Shen, H. Wang, J. Li, R. Huang, T. Yu, *FlexMat* **2024**, 1, 193. <https://doi.org/10.1002/flm2.24>